Consideration of Magnetic Dipole Orientation in Liquid Detected by Metallic Contaminants Detection System Using High-Tc SQUID

Saburo Tanaka, *Member, IEEE*, Masaru Sagawa, Kanji Hayashi, and Takeyoshi Ohtani

***Abstract*—The market for high-performance lithium-ion (Li-ion) batteries is growing rapidly as automobiles become electrified. The presence of small metallic particles of the order of 10 μm in a battery is likely to cause failure; therefore, it is important to eliminate them. We have developed a prototype system for detecting metallic foreign matter in liquid components for Li-ion batteries using a high-temperature superconducting radio-frequency superconducting quantum interference device, which is a highly sensitive magnetic sensor. Signal waveforms of a magnetized metallic piece passing through a trench located below the superconducting quantum interference device (SQUID) were measured. We found that the waveform depended on the direction of the magnetic dipole at the time of detection and could be roughly divided into six categories to explain all the experimental results. The maximum magnitude obtained for each sample was plotted against the equivalent spherical diameter of the sample. Our results indicate that the signal intensity was proportional to the cube of the sample diameter and that particles larger than $\phi 20 \times 30$ μm (equivalent spherical diameter 23 μm) were detected with signal-to-noise ratio $\geq$3.**

***Index Terms*—Contaminant detection, lithium-ion battery, liquid components, superconducting electronics, superconducting quantum interference device (SQUID).**

I. Introduction

With the electrification of automobiles, the market for high-performance batteries such as lithium-ion (Li-ion) batteries has been growing rapidly. The presence of small metallic particles of the order of 10 μm in a Li-ion battery can promote the growth of needle-like crystals and cause them to penetrate the separator that segregates the cathode and anode materials. This can result in a fire if the current is concentrated in the pinhole. To prevent such accidents, it is important both to evaluate the charge/discharge characteristics before shipment and to control the process to prevent metallic foreign matter from entering the product. We have developed a system for detecting metallic foreign matter in solids using a high-temperature superconducting (HTS) radio-frequency (RF) superconducting quantum interference device (SQUID), a type of ultrasensitive magnetic sensor, and we have recently been adapting this system for use in liquid components for batteries such as binders and slurries [1]–[4]. This has included evaluating the distance dependence of sensitivity by pulling a sample of the metallic foreign matter directly under the SQUID without flowing liquid [5].

In this article, the signals of metallic foreign particles in the water were detected by a SQUID installed outside the pipe while water was flowing, and the signals were examined. The relationship between the detected waveforms and the direction of the magnetic dipole is discussed in this article.

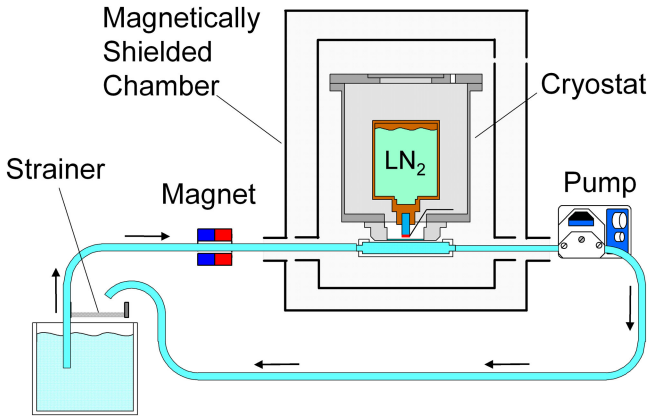

Fig. 1. System overview of the RF-SQUID-based metallic contaminant detection system. This prototype is a circulating system using a pump, with a strainer on the return side of the tank for collecting the metallic foreign matter sample.

II. Experimental

A. System Setup

1) Overview of the System: Fig. 1 shows a system overview of the HTS RF-SQUID-based metallic contaminant detection system. It is assumed that a liquid to be inspected for metal contamination is flowing in the tube. While the practical machine is designed to be inserted between processes, this prototype is a circulating system using a pump, with a strainer on the return side of the tank for collecting the metallic foreign matter sample. A permanent magnet (1.27 T) is positioned on the outside of

Manuscript received November 3, 2021; revised December 5, 2021; accepted December 9, 2021. Date of publication December 14, 2021; date of current version January 13, 2022. This article was recommended by Associate Editor J. Beyer. *(Corresponding author: Saburo Tanaka.)*

Saburo Tanaka and Kanji Hayashi are with the Toyohashi University of Technology, Toyohashi 441-8580, Japan (e-mail: tanakas@tut.jp; k153434@edu.imc.tut.ac.jp).

Masaru Sagawa is with the Sumitomo Electric Industries Ltd., Chuo-ku 107-8468, Japan (e-mail: m173413@edu.tut.ac.jp).

Takeyoshi Ohtani is with the Nikka Densok Limited, Kawagoe 350-1155, Japan (e-mail: otani@nikka-densok.co.jp).

Color versions of one or more figures in this article are available at https://doi.org/10.1109/TASC.2021.3135056.

Digital Object Identifier 10.1109/TASC.2021.3135056

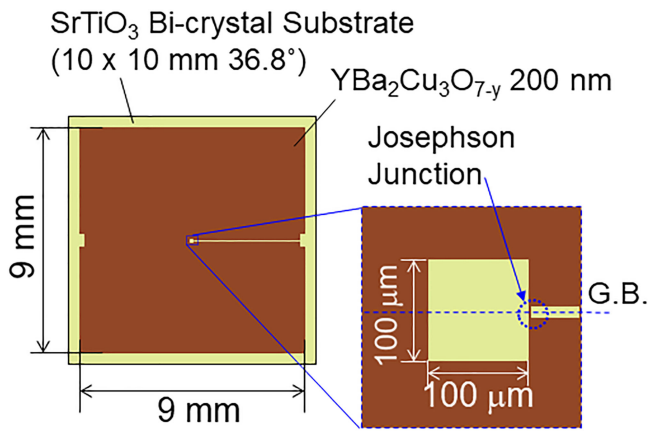

Fig. 2. Design of RF-SQUID magnetometer. The SQUID washer had an outer dimension of 9 × 9 mm square, with a 100 μm square hole in the center of the pattern. G.B. in the figure is an abbreviation for grain boundary.

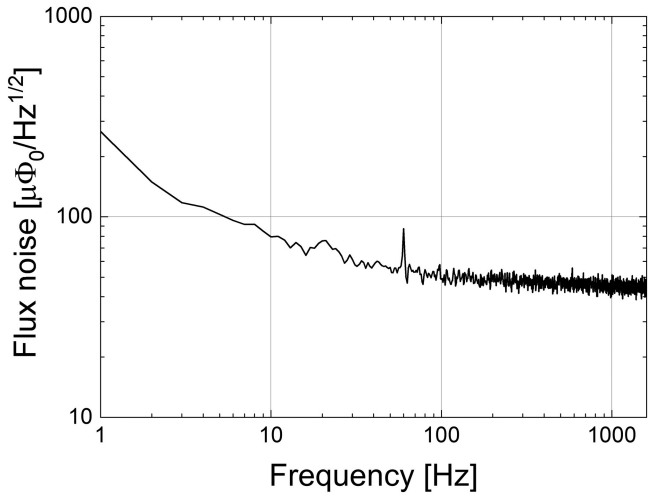

Fig. 3. Magnetic flux noise spectrum of RF-SQUID magnetometer. The white noise level was approximately 40 $\mu\Phi_0$/Hz$^{1/2}$, corresponding to field noise of 200 fT/Hz$^{1/2}$.

the tube. This magnetizes the metal contaminant, resulting in remanent magnetization that is detected by the RF-SQUID as the contaminant passes through.

2) RF-SQUID Magnetometer and Electronics: A design of the RF-SQUID magnetometer used in this study is shown in Fig. 2. $Y_1Ba_2Cu_3O_{7-y}$ (YBCO) thin film of 200 nm thickness was deposited on a $SrTiO_3$ bi-crystal substrate (10 × 10 × t0.5 mm^3, tilt angle: 36.8°), and an RF-SQUID pattern was formed on the film. The SQUID washer had an outer dimension of 9 × 9 mm square, with a 100 μm square hole in the center of the pattern. The SQUID inductance L_s and the effective area A_{eff} were estimated to be 157 pH and 0.40 mm^2, respectively [5].

The RF-SQUID was driven by electronics manufactured by Jülicher SQUID GmbH, Germany. The driving parameters were as follows: frequency f = 632 MHz, feedback resistance R_f = 6 kΩ, and integrator capacitor C = 4.7 nF. Fig. 3 shows the magnetic flux noise spectrum of the RF-SQUID. As shown in

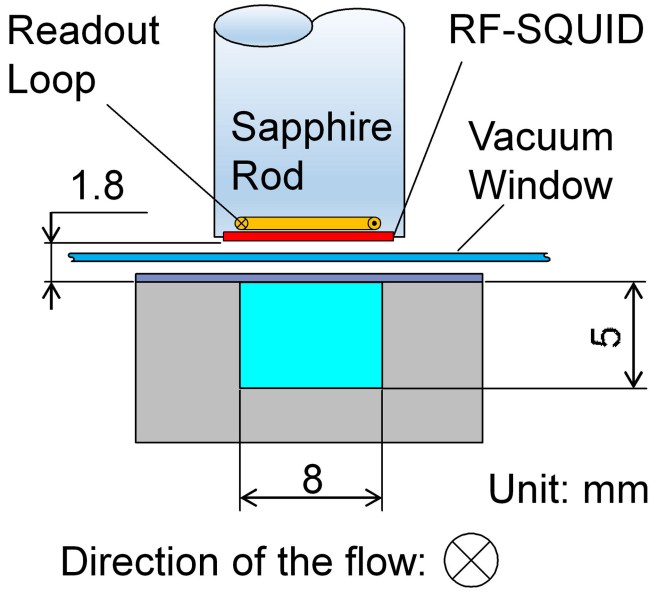

Fig. 4. Magnified view of the detection area. The spacing between the RF-SQUID surface and the inner wall of the trench was adjusted to be 1.8 mm (stand-off distance).

Fig. 3, the white noise level was approximately 40 $\mu\Phi_0$/Hz$^{1/2}$, corresponding to field noise of 200 fT/Hz$^{1/2}$.

The output signal from the SQUID electronics was passed through an analog filter set to remove noise components, and data were collected by a data acquisition unit. The cutoff frequencies f_c of the high-pass filter (HPF, 24 dB/Oct) and low-pass filter (LPF, 24 dB/Oct) were adjusted according to the flow velocity.

3) Cryostat and Vicinity of the Measurement Area: A specially designed cryostat was used to cool the RF-SQUID to liquid nitrogen temperature. The outer shell of the cryostat was a vacuum chamber made of aluminum alloy, and a copper tank (0.8 L) filled with liquid nitrogen was installed inside [6]–[8]. A sapphire thermal transfer rod was anchored to the bottom of the copper tank, and an RF-SQUID device was mounted on its tip. The RF-SQUID device was cooled to below the superconducting transition temperature via thermal conduction using sapphire, a nonmetallic material, to reduce the effect of Johnson–Nyquist noise caused by thermal fluctuations of free electrons in the metal.

The bottom of the cryostat was sealed by a 0.5-mm-thick sapphire vacuum window. The distance between the vacuum window and the RF-SQUID device was 0.5 mm, allowing for the distance between the RF-SQUID in the vacuum chamber and the atmosphere outside the cryostat to be as small as possible (see Fig. 4). The dimensions of the trench were W8 × D5 mm. When assembling the experimental system, the spacing between the RF-SQUID surface and the inner wall of the trench was adjusted to be as close as 1.8 mm (stand-off distance). With a washer size of 9 × 9 mm^2, the RF-SQUID approximately covers the 8-mm-wide trench, considering the stand-off distance of 1.8 mm.

4) Magnet and Magnetic Shield Design: To magnetize the foreign sample, a permanent magnet generating a magnetic

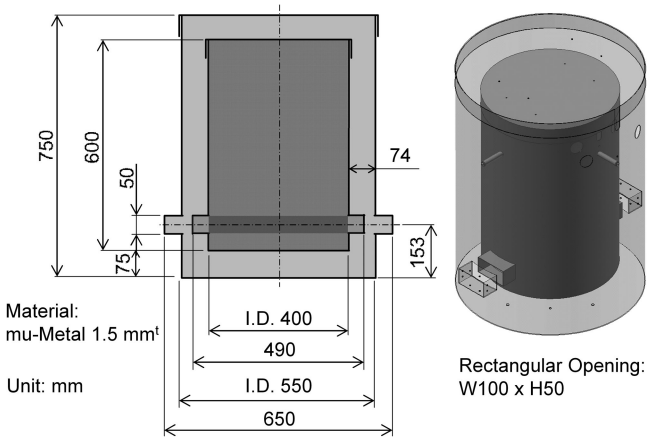

Fig. 5. Magnetic shield design. Shield was constructed from permalloy (mu-metal) with a thickness of 1.5 mm.

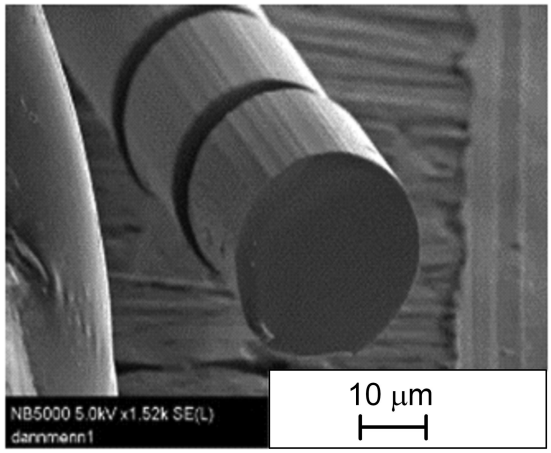

Fig. 6. Micrograph of wire cut sample. SUS304 stainless steel wires were cut using a Ga-FIB.

field parallel to the flow direction was installed. The external dimensions of the magnet were W140 × H90 × D60 mm, and the size of the opening through which the tube passed was W100 × H10 mm. The measured magnetic flux density at the center of the magnet was 1.27 T.

We designed a two-layered cylindrical magnetic shield for use in a detection system (illustrated in Fig. 5). The shield was constructed from permalloy (mu-metal) with a thickness of 1.5 mm. The dimensions of the outer layer were set to ϕ550 × 750 mm (inner diameter × height), and those of the inner layer were ϕ400 × 600 mm (diameter × height). As shown in Fig. 5, sleeved openings of 100 mm in width and 50 mm in height were included on the sides of the outer and inner layers. The center of the rectangular cross section of the opening was 153 mm from the bottom of the shield, and the length of the sleeves for both the inner and outer layers was 50 mm [9]. The vertical and diametrical interlayer spacing between the outer and inner layers was set to 75 and 74 mm, respectively.

For these design parameters, the shielding factor (SF), which is a performance indicator of magnetic shielding, was obtained using the electromagnetic field analysis software ANSYS Maxwell 3D. In the simulation, the magnitude of the applied static magnetic field was set to 50 μT, equivalent to that of the geomagnetic field. The magnitude of the magnetic field at the center of the SQUID was investigated under the assumption that the magnetic field was applied in the direction of the SQUID sensitivity axis (*Z* direction) and in the direction of foreign object movement (*X* direction) of the magnetic shield. The SF values on the application of the magnetic field for each axis were 657, 2.4×10^6, and 178 for B_x, B_y, and B_z, respectively.

B. Sample Preparation

We searched for spherical samples that would simulate magnetic metallic foreign particles with diameters of 20–50 μm, but there were no equivalent products on the market; therefore, we decided to fabricate our samples. We prepared SUS304 stainless steel wires (*Nilaco Corporation*, Cr18% – Ni8% – Fe) of several diameters and cut them using a gallium-focused ion beam (Ga-FIB). The wire diameters were ϕ50, ϕ30, and ϕ20 μm. SUS304 is a commonly used material in battery manufacturing equipment. It is austenitic stainless steel that does not exhibit magnetism; however, when stress is applied, a part of its structure transforms into martensite, which exhibits ferromagnetism [10]. It is expected that the generation of metallic foreign bodies in actual manufacturing sites is caused by the wear and fatigue of metallic parts, which are often subjected to stress. Therefore, it is assumed that the internal structure of metallic foreign particles is transformed into a martensitic structure, which can be detected using remanent magnetization detection methods. Fig. 6 shows a micrograph of a ϕ30 × L30 μm piece of wire after being cut by Ga-FIB. As the cut wire pieces were extremely small and difficult to handle, they were picked up and embedded in UV-curing resin (*Bondic BD-CRJ*) to make hemispherical samples with a diameter of approximately 1–2 mm [6].

III. Experimental Results and Discussion

A. Effect of Filtering

A molded SUS304 sample with dimensions ϕ50 × L50 μm was propelled through a water stream by a pump with a flow rate of 33 m/min. The sample was magnetized as it passed through the permanent magnet, and the remanent magnetization was detected by the HTS RF-SQUID. Fig. 7 shows the time traces of the detected signal. The flux-to-voltage conversion factor was 5.5 ϕ_0/V. The upper waveform shows the signal without a filter, and the lower waveform is with a filter. The upper waveform in the figure has been offset for clarity. The cutoff frequencies (f_c) of the HPF and LPF were set to 10 and 100 Hz, respectively. These results show that applying the filter significantly reduced the noise, thus improving the signal-to-noise ratio (SNR).

B. Variation of Signals

We measured the remanent magnetization of a ϕ30 × L30 μm sample in a water flow as above and repeated the same process using RF-SQUID, with HPF and LPF applied. Fig. 8(1)–(8)

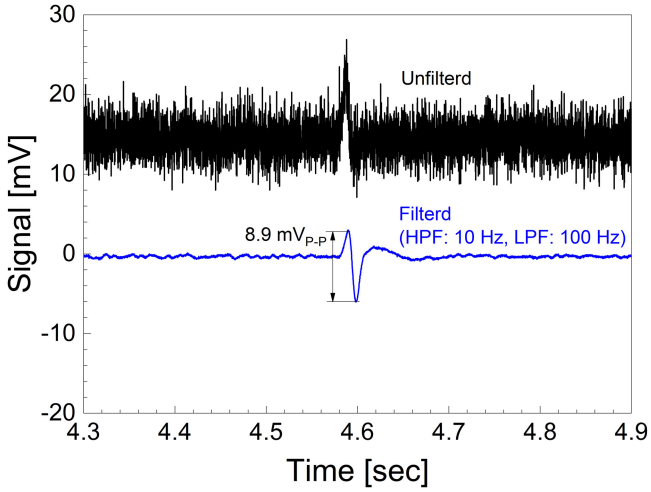

Fig. 7. Time traces of the detected signals. The upper waveform is without filter and the lower is with filter. The upper waveform has been offset for clarity.

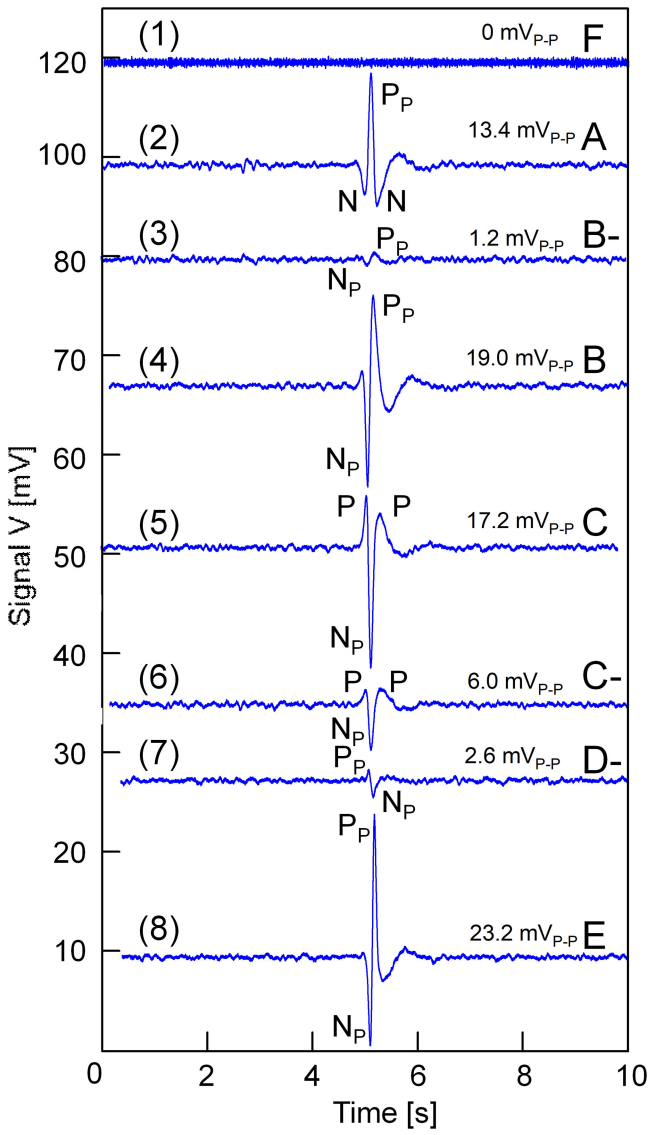

Fig. 8. Time traces for each repetition, arranged in measurement order. Flux-to-voltage conversion factor was 5.5 ϕ_0/V. Waveforms have been offset for clarity.

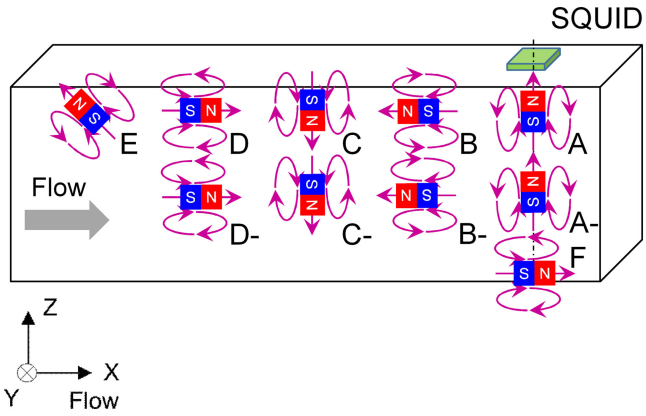

Fig. 9. Orientation of magnetic dipoles in trench. Orientation of the magnetic dipoles can be roughly divided into six categories from A to F.

shows the time traces for each repetition, arranged in measurement order. The waveforms in the figure have been offset for clarity. Each peak-to-peak value is shown in the figure as a unit of mVp-p. The signal waveforms have various shapes, and the peak-to-peak values vary across the range 0–23.2 mV, with variation seeming to depend on the positional relationship between the sample and the SQUID. As shown in Fig. 4, the SQUID approximately covers the width of the trench, meaning that the dependence in the width direction is small whereas that in the depth direction is large. The signal is expected to be smaller when the sample passes far from the SQUID and larger when it passes near it. In Fig. 8, the shapes can be classified into six major categories. In (1), there is no signal, and the sample is expected to have passed extremely far from the SQUID. (2) can be expressed as negative, positive peak, and negative (N-P_P-N). (5) and (6) are P-N_P-P, indicating that the polarity is reversed from (2). In (4), there are large peaks at both the positive and negative poles, resulting in N_P-P_P, and (7) is small but with polarity reversed (P_P-N_P). We consider the last negative bump in (4) to be an effect of the delay caused by the time constant of the HPF; thus, it is ignored. (8) shows N_P-P_P with the same shape as (4), but the negative peak is smaller than the positive peak by approximately 50%, resulting in an unbalanced shape.

C Orientation of Magnetic Dipoles

Assuming that the magnetization by the permanent magnet is constant, the peak-to-peak value of the signal depends on the positional relationship between the sample and the SQUID, as described above: the signal becomes smaller when it is farther from the SQUID and larger when it is closer. The signal waveform itself is expected to depend on the direction of the magnetic dipole when the magnetized metallic particle passes under the SQUID. As shown in Fig. 9, the orientation of the magnetic dipoles can be roughly divided into six categories, A–F. A and C are perpendicular to the SQUID sensitive plane, B and D are horizontal, and E is on a diagonal axis. A-, B-, C-, and D- have the same orientation as A, B, C, and D, respectively, but are a little farther from the SQUID. In these cases, the signal strength is smaller. F shows the case where the magnetic dipole passes

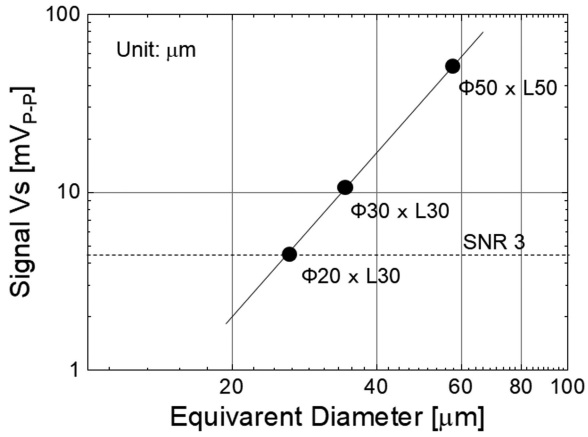

Fig. 10. Dependence of voltage on particle spherical equivalent diameter. Each sample was measured ten times, and the maximum value for each was plotted as the equivalent spherical diameter.

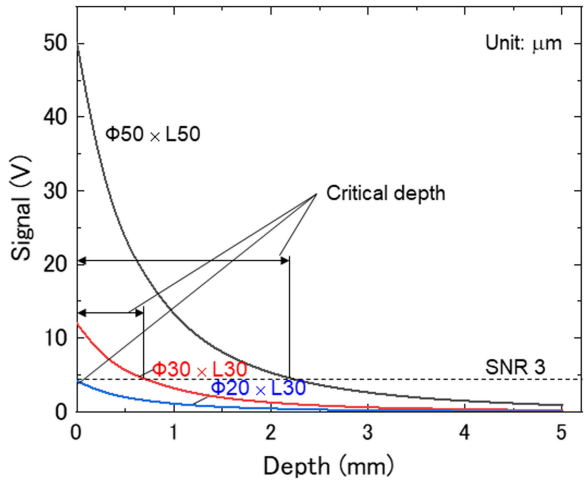

Fig. 11. Dependence of signal on depth (calculation). Assuming a detection limit of SNR 3, the critical depth was 2.2 mm for ϕ50 $\times$ L50 μm, 0.7 mm for ϕ30 $\times$ L30 μm, and 0 mm (the top of the trench) for ϕ20 $\times$ L30 μm.

near the bottom of the trench far from the SQUID, and no signal is detected. We note that the orientations of the dipoles in E and F are representative and various orientations can be assumed. If we add the four from A- to D-, the total number of categories becomes 10. We can classify all the waveforms in the categories shown on the right-hand side in Fig. 8.

D. Dependence of Particle Diameter

We prepared samples of three different sizes and conducted detection experiments in the same manner. As mentioned in Section III-B, the magnitude and waveform of the signal varied significantly between different measurements, even for the same sample. Therefore, each sample was measured ten times, and the maximum value for each was plotted against the equivalent spherical diameter. As the samples were cylindrical, the equivalent spherical diameter was calculated from the diameter of each sample based on its volume. Fig. 10 shows the dependence of the maximum signal (peak-to-peak value) on the equivalent diameter. The signal intensity is proportional to the cube of the equivalent diameter; in other words, it is proportional to the volume. The dashed line in the figure indicates an SNR level of 3. These results show that particles larger than ϕ20 $\times$ L30 μm (equivalent spherical diameter of ϕ23 μm) were detected at SNR $\geq$3.

E. Dependence of Depth

The peak-to-peak value of the signal depends on the distance between the sample and the SQUID, which is inversely proportional to the cube of the distance [11]. We calculated the dependence of the signal on the depth (from the top of the trench to the bottom) for the three metal samples of different sizes. It was assumed that the maximum value would be obtained when the sample was closest to the SQUID (stand-off distance of 1.8 mm; see Fig. 4). The signal's proportionality to the cube of the equivalent diameter, as shown in Fig. 10, supports this assumption. The depth dependence results are shown in Fig. 11. The depth was defined as the distance from the SQUID to the sample minus the stand-off distance of 1.8 mm, with the top of the trench as zero. We used the largest signal amplitude obtained in ten repeated measurements as the value at zero depth. The signal decayed as the depth that the sample passed through increased. Assuming a detection limit of SNR 3, the critical depth was 2.2 mm for ϕ50 $\times$ L50 μm, 0.7 mm for ϕ30 $\times$ L30 μm, and 0 mm (the top of the trench) for ϕ20 $\times$ L30 μm.

To increase the critical depth, the stand-off distance of the SQUID should be further reduced to $<$1 mm. It is also important to reduce the SNR 3 level by improving the magnetic flux noise of the SQUID with bandwidth between 10 and 100 Hz. Another option is to prepare several SQUIDs and place them around the trench [5].

IV. Conclusion

In this article, we have developed a prototype system for detecting metallic foreign particles in the liquid components of Li-ion batteries using an HTS RF-SQUID. For the experiment, SUS304 wires were cut using Ga-FIB to prepare small metal samples of sizes ranging from approximately ϕ20 to ϕ50 μm. The samples were propelled through a water flow, and the signal of the metal particles in the water was detected using a SQUID installed outside the pipe. When the same experiment was repeated, the signal strength varied and was sometimes reduced to zero. Furthermore, a different waveform was produced each time. From our investigation, we found that the variation in signal strength depended on the distance from the SQUID to the sample, whereas the waveform depended on the direction of the magnetic dipole at the time of detection and could be roughly divided into six categories that could explain all the experimental results.

When the maximum magnitude obtained for each sample was plotted against the equivalent spherical diameter of the sample, the signal intensity was shown to be proportional to the cube of the sample equivalent diameter, and we found that particles larger than ϕ20 $\times$ L30 μm (23 μm in equivalent diameter) were detected with SNR $\geq$3. Furthermore, assuming that the signal

strength is inversely proportional to the cube of the distance, we calculated the critical trench depth at which the samples could be detected as 0.7 mm for $\phi 30 \times$ L30 μm.

In the future, it is necessary to increase the critical depth for practical use by reducing the stand-off distance and the noise in the SQUID bandwidth of 10–100 Hz. The current level is 50–100 $\mu\phi_0/\mathrm{Hz}^{1/2}$; therefore, there should be sufficient margin to reduce the noise.

REFERENCES

[1] S. Tanaka *et al.*, "High-T_c SQUID detection system for contaminants in food and drug," *Chin. J. Phys.,* vol. 42, pp. 526–533, 2004.

[2] M. Bick *et al.*, "A SQUID-based metal detector: Comparison to coil and X-ray systems," *Supercond. Sci. Technol.,* vol. 18, pp. 346–351, 2005.

[3] H. J. Krause *et al.*, "Detection of magnetic contaminations in industrial products using HTS SQUIDs," *IEEE Trans. Appl. Supercond.,* vol. 15, no. 2, pp. 729–732, Jun. 2005.

[4] S. Tanaka, T. Ohtani, Y. Uchida, Y. Hatsukade, and S. Suzuki, "Contaminant detection system using high T_c SQUID for inspection of lithium ion battery cathode sheet," *IEICE Trans. Electron.,* vol. E98-C, pp. 174–177, 2015.

[5] S. Tanaka, M. Sagawa, K. Hayashi, and T. Ohtani, "Development of metallic contaminant inspection system using high-T_c rf-SQUID for Li-ion battery liquid components," *IEEE Trans. Appl. Supercond.,* vol. 30, no. 7, Oct. 2020, Art. no. 1600604.

[6] M. Sagawa, K. Hayashi, T. Ohtani, and S. Tanaka, "Metallic contaminant detection in liquids using a high-T_c RF-SQUID," *J. Phys. Conf. Ser.,* vol. 1975, 2021, Art. no. 012021_1-4.

[7] T. S. Lee, G. Dantsker, and J. Clarke, "High-transition temperature SQUID microscope," *Rev. Sci. Inst.*, vol. 67, 1996, Art. no. 4208.

[8] S. Tanaka, O. Yamazaki, R. Shimizu, and Y. Saito, "High-T_c SQUID microscope with sample chamber," *Supercond. Sci. Technol.*, vol. 12, pp. 809–812, 1999.

[9] S. Tanaka, Y. Hatsukade, T. Ohtani, and S. Suzuki, "SQUID sensor application for small metallic particle detection," *J. Magnetism Magn. Mater.*, vol. 321, pp. 880–883, 2009.

[10] H. Huang, J. Ding, and P. G. Mccormick, "Microstructural evolution of 304 stainless steel during mechanical milling," *Mater. Sci. Eng.,* vol. A-216, no. 1-2, pp. 178–184, 1996.

[11] S. Tanaka, T. Ohtani, and H.-J. Krause, "Prototype of multi-channel high-T_c SQUID metallic contaminant detector for large sized packaged food," *IEICE Trans. Electron.,* vol. E100–C, pp. 269–273, 2017.

Saburo Tanaka (Member, IEEE) received the B.E. and M.E. degrees in electrical and electronic engineering from the Toyohashi University of Technology, Toyohashi, Japan, in 1981, and 1983, respectively. He received the Doctoral degree in engineering from Osaka University, Suita, Japan, in 1991.

Since 1987, he has been involved in the research of high-temperature superconductors with Sumitomo Electric Itami Research Laboratory. He was engaged in the development of multichannel high-T_c SQUID systems at the Superconducting Sensor Laboratory from 1991 to 1995. He was a Visiting Research Associate with the Department of Physics, University of California at Berkeley from 1996 to 1997. He is currently a Professor and Vice President with the Toyohashi University of Technology.

Dr. Tanaka is a member of the Japan Society of Applied Physics, the Institute of Electronics, Information and Communication Engineers, and the Institute of Electrical Engineers of Japan.

Masaru Sagawa received the M.E. degree in applied chemistry and life science from the Toyohashi University of Technology, Toyohashi, Japan, in 2021.

He is currently working with Sumitomo Electric Industries Ltd., Japan, Osaka, Japan. His research interest includes the development of contaminant detection system using HTS SQUID.

Kanji Hayashi received the B.E. and M.E degrees in environmental and life sciences from the Toyohashi University of Technology, Toyohashi, Japan, in 2017 and 2019, respectively. He is currently working toward the Ph.D. degree in applied chemistry and life sciences with the Toyohashi University of Technology.

Takeyoshi Ohtani received the graduate degree from Jishukan High School, Toyohashi, Japan, in 1989.

He joined RD Department of Advance Food Technology Company, Ltd. in 2002. He was engaged in the development of a contaminant detection system using high-T_c SQUIDs from 2002. He is currently a Researcher with Nikka Densoku Limited. He was engaged in priority research project of "Knowledge Hub Aichi" since 2012.

He is a member of the Japan Society of Applied Physics.